Exploring the Earth

NORSAR Scientific Report No.1-2014

Semiannual Technical Summary

1 January – 30 June 2014

Tormod Kværna (Ed.)

Kjeller, December 2014

NORSAR

6.3 Reflectivity versus ray-tracing in infrasound propagation modelling

6.3.1 Abstract

This work considers infrasound propagation modelling. We compare results obtained using a classical ray-tracing program with results produced by the reflectivity method. The reflectivity method is applied widely by the seismological community to generate synthetic seismograms for elastic waves propagating in a stratified earth. However, to the best of the authors' knowledge, there has not been any previous comparison between ray-tracing and the reflectivity method for modelling the propagation of observed infrasound signals.

We apply a ray-tracing engine and a reflectivity code to the atmospheric conditions along the great circle path which connects the Drevja accidental explosion on December 17, 2013 and the IS37 infrasound array station near Bardufoss, Troms, Norway. The modelling results are compared with the observed signals recorded at the array.

6.3.2 Background

On December 17, 2013, a truck with 15 tons of slurry, to be used for road construction, exploded near the settlement of Drevja in the Nordland region of Norway. This event was considered also in Näsholm (2014). The origin time is estimated from local eyewitnesses to be 2013-351:14.26 and the coordinates are 65.988°N, 13.343°E. Signals from this event were observed at all of the Nordic infrasound arrays, and propagation paths to different stations observing the event are shown in Figure 6.3.1. The signals considered in the current work are recorded at the IS37 array which is situated around 410 km from Drevja.

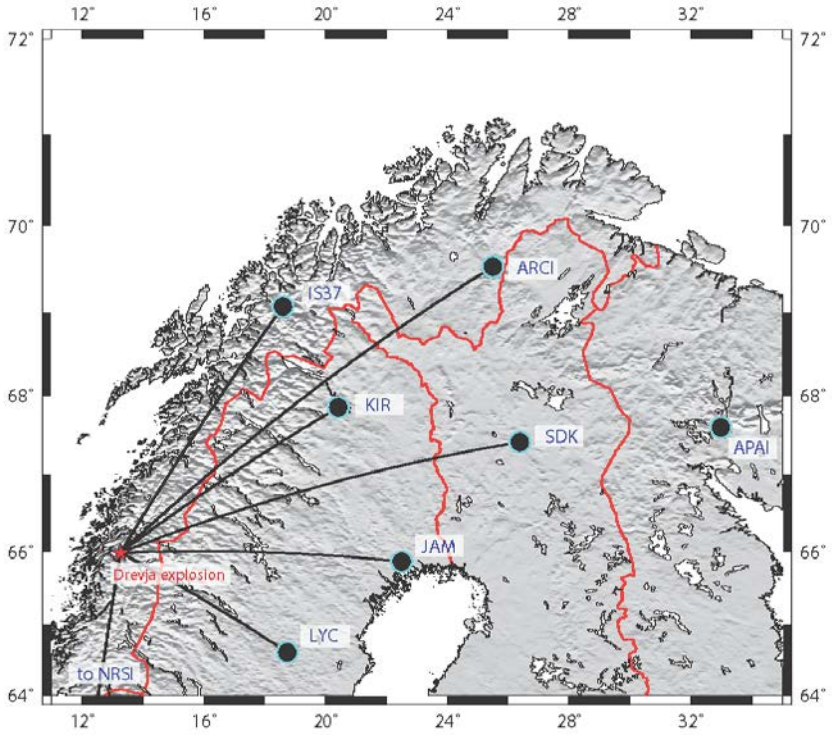

Fig. 6.3.1 Location of the Drevja accidental explosion in relation to infrasound arrays in the region.

6.3.3 Atmospheric model

The sound speed and winds applied from 0 to 75 km altitude are the GEOS5/MERRA public profiles published by NASA. Above this altitude, the profiles are compiled from the empirical NRLMSISE-00 (temperature) and HWM07 (wind) empirical models. The profiles at the location of the event and at the IS37 array are shown in Figure 6.3.2.

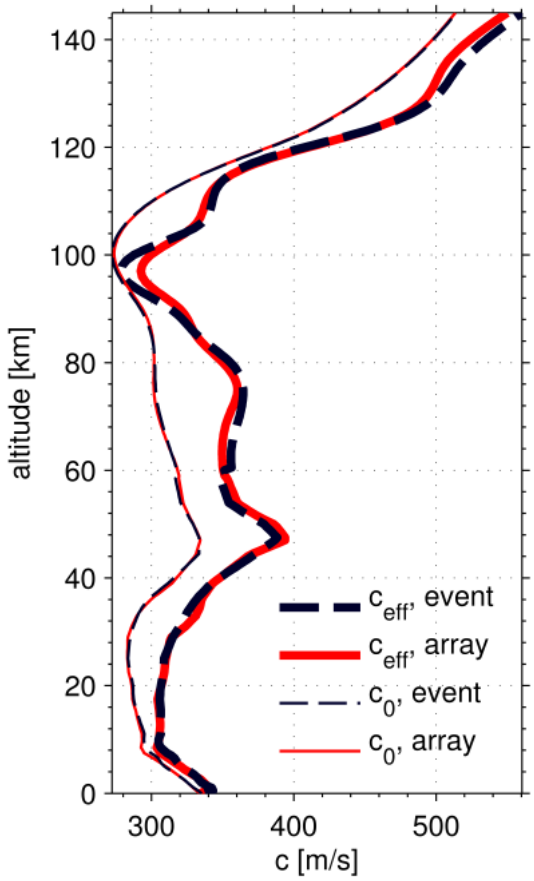

Fig. 6.3.2
Adiabatic sound speed as well as effective sound speed profiles at the event and at the IS37 array

6.3.4 Modelling approaches

We compare the following 4 modelling approaches for propagation of signals from Drevja to the IS37 array:

(A.) **ART2D ray-tracing with separated temperature and wind effects**
Ray-tracing using the ART2D code, while taking full advantage of its possibility to take wind effects into account separately from the sound speed. The sound speed is modeled in an anisotropic manner.

(B.) **Range-independent ART2D ray-tracing with separated temperature and wind effects**
Ray-tracing using the ART2D code, while taking full advantage of its possibility to take wind effects into account as in (A). However this approach incorporates no range-dependence of the atmosphere. The profile above the event is applied along the whole great circle.

(C.) **Range-independent, $c_{effective}$ ART2D ray-tracing**
Ray-tracing using the ART2D code, with range-independent atmospheric specifications (as in (B)). However, in this approach, wind effects are included only by constructing an effective speed of sound $c_{effective} \equiv c_0 + c_w$, where c_0 is the adiabatic temperature-dependent speed and c_w is the

projection of the wind speed in the direction along the great circle between the event and the array. The atmospheric model along the great circle is hence both range-independent and equal for any elevation angle in the propagation direction.

(D.) **Range-independent, $c_{effective}$ reflectivity modelling**

Application of the full waveform modelling reflectivity method (Müller, 1985) for a pulse within the same range-independent $c_{effective}$ medium as in method (C). In gas, only one type of elastic waves can propagate: the compressional wave. This purely acoustic wave propagation can be modelled simplistically with a pure SH-wave propagation code, but using the compressional wave velocities and the density of the atmosphere as the propagation model. For this application, the geometry of the original SH-code of G. Müller has been modified by letting the atmosphere be the modelled medium and the solid Earth correspond to the upper half-space in the original code. Also, the Earth-flattening approximation is adjusted to take a spherical atmosphere into account. The absolute amplitudes resulting from this modelling cannot be used since the code was written for displacements and the observations are pressure changes. However, the relative amplitude changes of the different phases should be correct. Figures 6.3.3, 6.3.4 and 6.3.5 illustrate the modelling results using ray-tracing approaches (A) – (C). Figure 6.3.6 illustrates the modelling arrival ground hit times using ray-tracing approaches (A) – (C) in comparison with the traces generated by the reflectivity method.

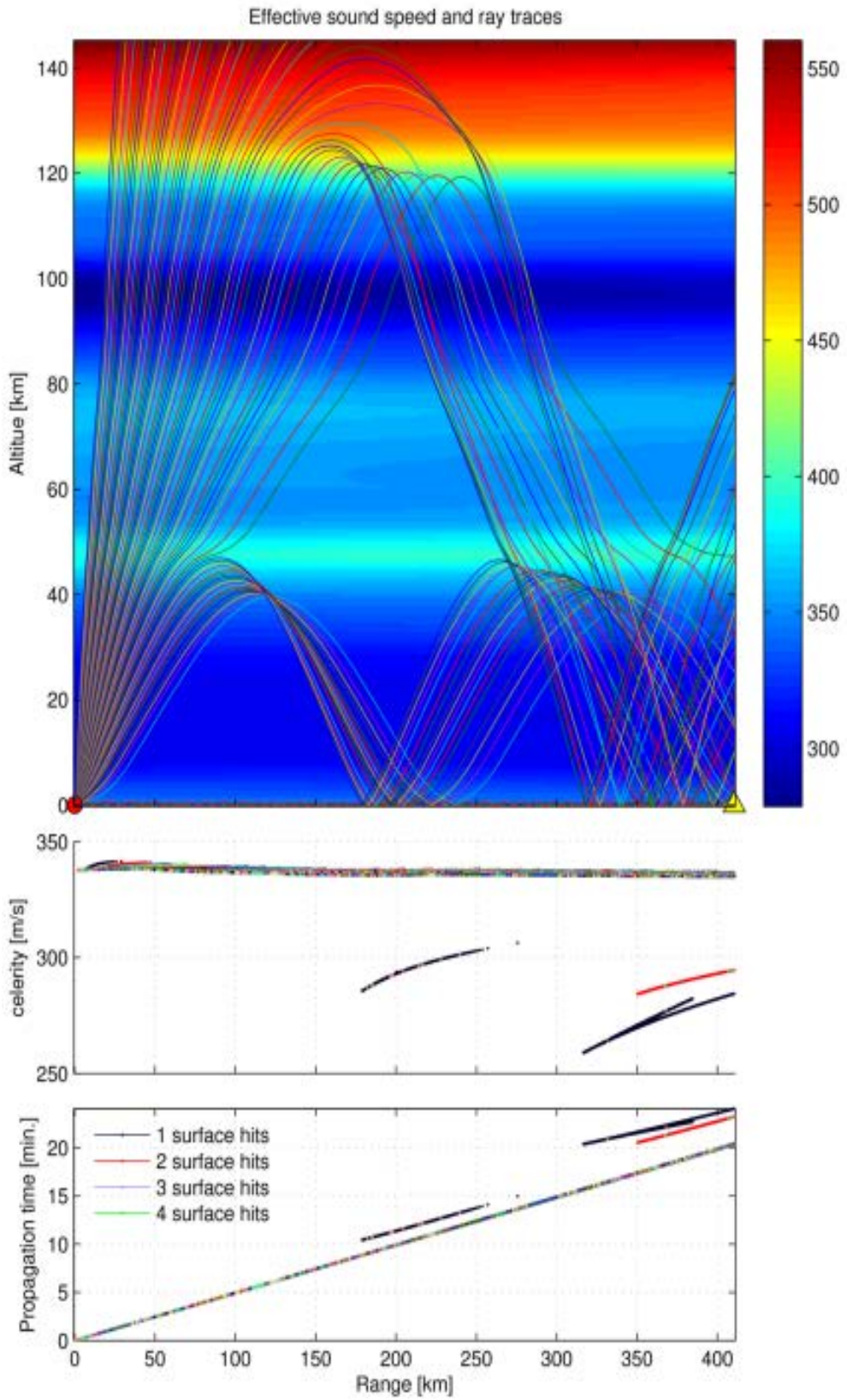

Fig. 6.3.3. Ray-tracing results using approach (A): ART2D ray-tracing with separated temperature and wind effects.

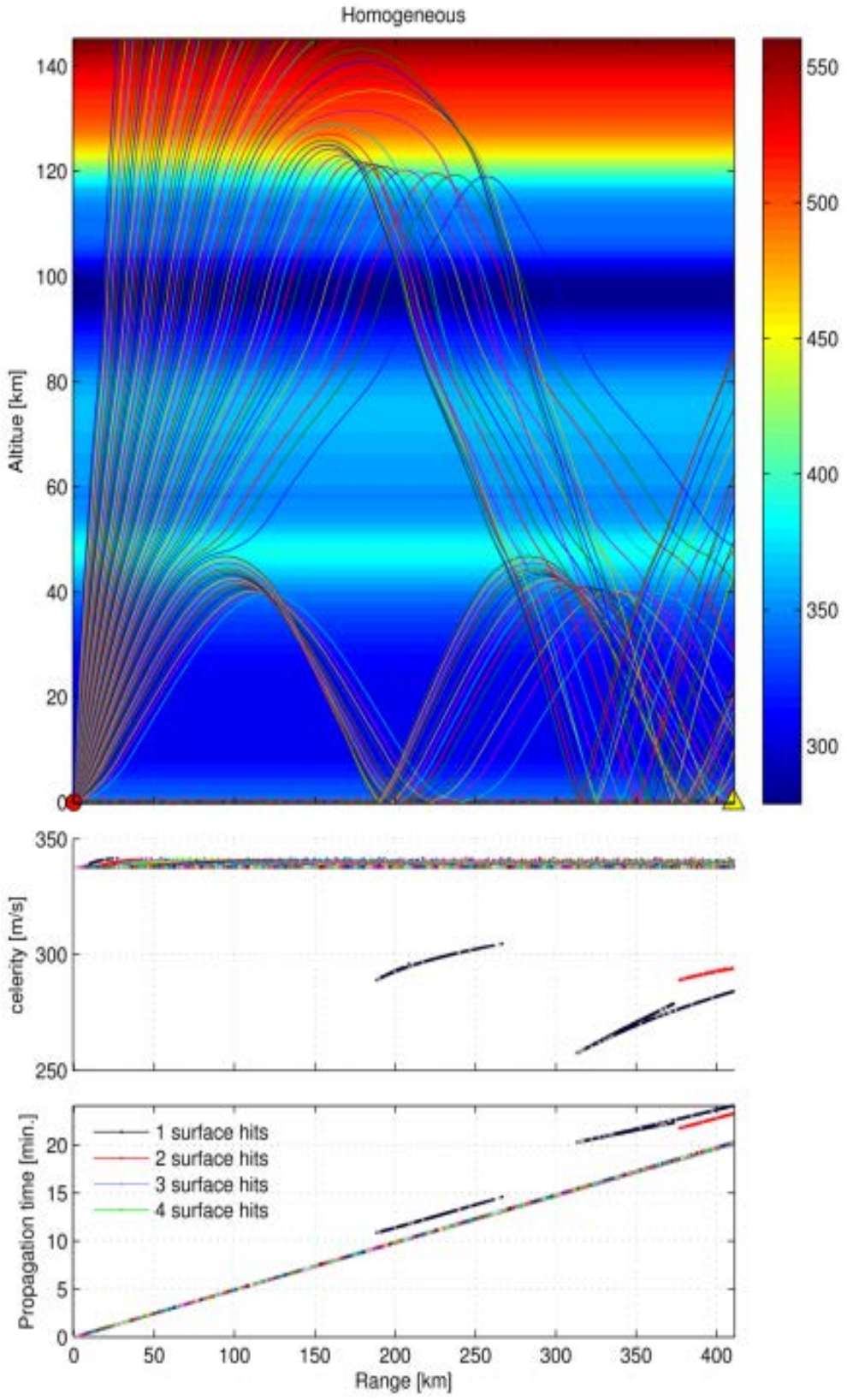

Fig. 6.3.4. Ray-tracing results using approach (B): Range-independent ART2D ray-tracing with separated temperature and wind effects.

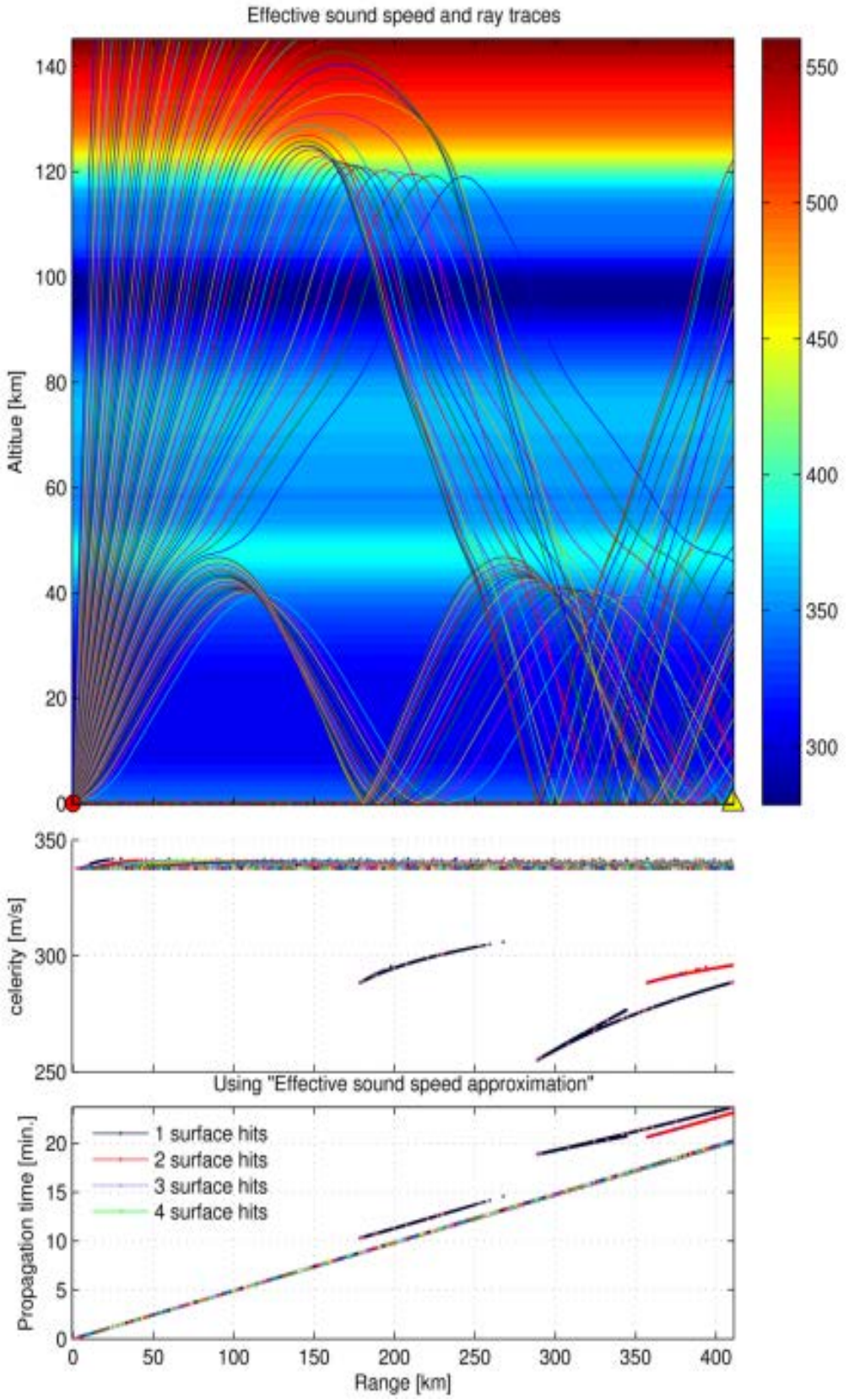

Fig. 6.3.5. Ray-tracing results using approach (C): Range-independent, $c_{effective}$ ART2D ray-tracing where wind effects are accounted for using the $c_{effective}$ approach

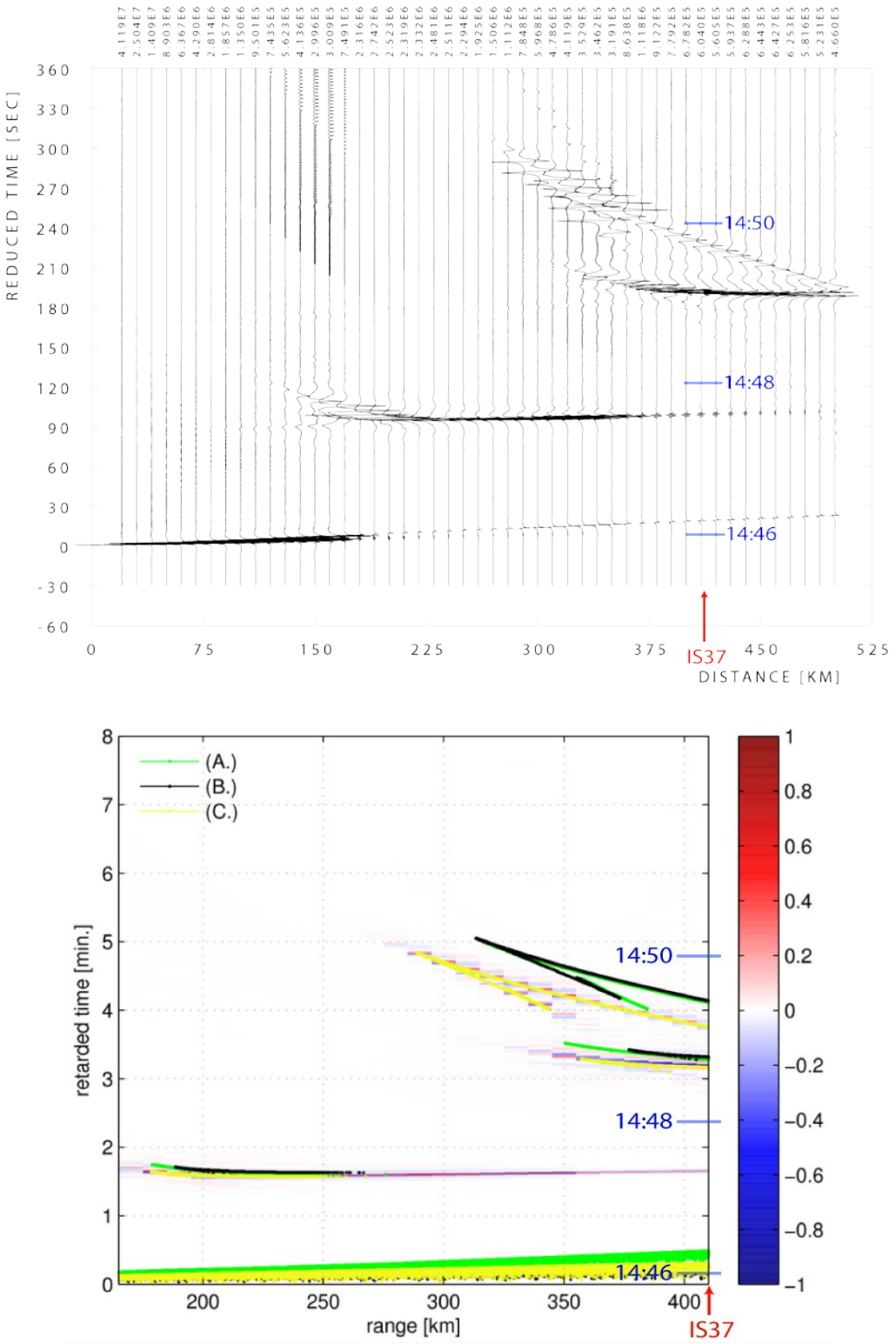

Fig. 6.3.6. Top panel: Signal traces generated by the reflectivity method. The reduced time velocity is 0.343 km/s. The signal dominant frequency is 2 Hz, while the calculation frequency range is 0.1 – 4 Hz sampled at 20 Hz. Each trace is normalized by a factor displayed in the top row. Bottom panel: The ray-tracing ground hit times from method (A), (B), and (C) overlaid on the color-coded amplitudes generated by the reflectivity method (D). The sensor array is located at a range of 410 km, as indicated by red arrows. The blue lines indicate the UTC times 14:46, 14:48, and 14:50 at the range of IS37.

6.3.5 Observed infrasound signals compared with modelling results

Figure 6.3.7 illustrates the signals recorded on the 10 sensors of IS37 in the frequency band 1-6 Hz. The high-frequency content of these signals, having propagated a distance over land of over 400 km, is significant. The signal-to-noise ratio (SNR) below 2 Hz is very low, and is far superior in the 2-5 Hz band. Such events demonstrate how useful the geometrical design of the array is with the innermost ring of closely spaced elements which allow the direction and apparent velocity of high frequency signals to be estimated.

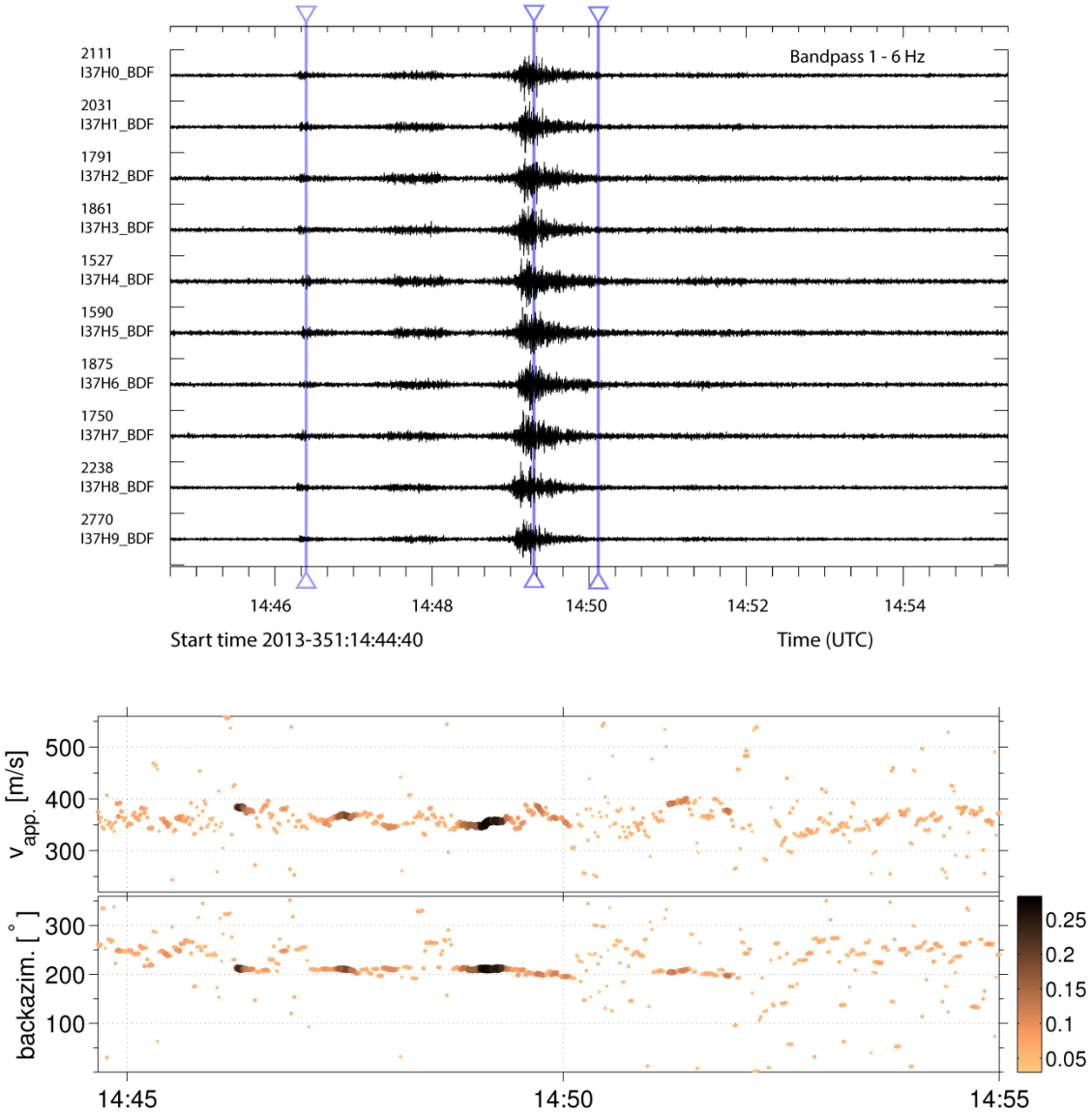

Fig. 6.3.7. Top panel: Waveforms recorded at IS37 with phase arrivals estimated by ART2D ray-tracing (approach A – Figure 6.3.3) indicated by blue vertical lines. Bottom panel: The corresponding apparent velocity and back-azimuth from f-k analysis.

6.3.6 Discussion

Observed tropospheric and stratospheric phases predicted by ray-tracing and reflectivity

The full ray-tracing (approach A – Figure 6.3.3) predicts three distinct infrasound phase arrivals at ground level at the IS37 array range: first a tropospheric arrival (at ~14:46 UTC), then a stratospheric arrival (at ~14:40.30), and finally a thermospheric arrival (at ~14:49.30).

The reflectivity modelling (Figure 6.3.6) predicts these tropospheric, stratospheric, and thermospheric arrivals. Also, an additional stratospheric arrival is present in the modelled traces, as discussed in the next subsection.

Looking at the observed waveforms in Figure 6.3.7, where the phase arrivals estimated by ray-tracing are indicated by vertical lines, we note that the first ray-tracing arrival estimate agrees with a received low-amplitude signal. The corresponding apparent velocity and back-azimuth from f-k analysis (shown below the waveforms) suggests that this is a tropospheric or stratospheric arrival from the direction of the event. Similarly, the second predicted ray-tracing arrival corresponds well with an observed high-amplitude signal.

Observed stratospheric phase predicted by reflectivity but not by ray-tracing

The data also reveal a phase arrival at around 14h47. This phase is not predicted by the ray-tracing procedure, but is anticipated by the reflectivity method as illustrated in Figure 6.3.6 (the phase arriving at the 410 km range at around 90s in reduced time). On the other hand, we see that the "first-bounce" arrivals predicted by ray-tracing within the approximate range interval [175, 275] km coincide with ones predicted by the reflectivity method (D). If we now in Figure 6.3.6 "extrapolate" these ray-tracing predictions all the way to the array location, we see that we are in line with both the reflectivity method predicted phase arrival and the phase observed in the collected data. Ray-trace modelling methods cannot predict such *head wave* phenomena.

Thermospheric phases

A thermospheric arrival is predicted by both the ray-tracing and the reflectivity modelling. But the arrival times of these predictions does not correspond with a signal visible in the data traces, nor with an increase in coherence between the elements.

However, looking at Figure 6.3.7 later in the data (at around 14:52 UTC), we can see a (very) slight "stabilization" of the backazimuth and apparent velocity estimates which might indicate the arrival of a weak thermospheric signal at the array.

Range-independence and $c_{effective}$ approximations

Figure 6.3.6 also illustrates that the ray-tracing methods (A) and (B) in this example provide very similar phase arrival times, hence indicating that the range-independent assumption is appropriate for modelling Drevja signal arrivals at IS37. On the other hand, the thermospheric and stratospheric phase arrival times predicted by ray-tracing with condition prescribed for approach (C) differ from the ones predicted by ray-tracing with the conditions prescribed for approaches (A) and (B), most significantly for the thermospheric arrivals. This is in line with the assumption that the greater the vertical portion of the ray propagation path is, the more the $c_{\text{effective}}$ assumption should deviate from

the true wind speed influence, which has to be taken in the true direction of propagation. The ray-tracing approach (C) uses the same range-independent $c_{effective}$ assumption as the reflectivity method (D). It is therefore intuitive that the phase arrivals predicted using (C) coincide with high pulse amplitudes calculated using (D).

6.3.7 Concluding remarks

By applying reflectivity modelling, we can avoid some limitations of conventional ray-tracing, e.g., we can get better head wave representation and less pronounced shadow zones. This is illustrated in our Drevja explosion example: the reflectivity method predicts a phase arriving at the station after turning only once in the stratosphere while ray-tracing does not predict this phase (which is observed in the recorded signals).

There are seismic modelling codes which model anisotropic velocity, and we intend to test these out for infrasound propagation. We foresee to more accurately model wind effects, hence avoiding disadvantages appearing due to the $c_{effective}$ approximation that we had to apply in the reflectivity modelling described in the current work.

References

Müller, G. (1985). The reflectivity method: a tutorial. J. Geophysics **58**, 153-174.

Näsholm, S.P (2014). Infrasound signal detection from the Drevja accidental explosion, Chapter 6.2, NORSAR Scientific Report **2-2013**, Semiannual Technical Summary, 1 July – 31 December 2013, (ed. Tormod Kværna), pp. 40-50.

Walker K. (2012). Atmospheric ray tracer 2D (ART2D). See the URL http://sail.ucsd.edu/~walker/software/ART2D/art2d.html

S. P. Näsholm, NORSAR
J. Schweitzer, NORSAR
T. Kværna, NORSAR
S. J. Gibbons, NORSAR